Rip Currents and Rip Channel Morphodynamics under Quasi-Steady Conditions

Julian Simeonov, Todd Holland, Steven Spansel
Marine Geosciences, Naval Research Laboratory, Code 7440.3,
Stennis Space Center, MS 39529, USA

***Abstract*-We developed a realistic test case for morphodynamic predictions of short-term bathymetry evolution associated with quasi-steady rip currents. Assuming stationary forcing, predictions made by the coupled wave-hydrodynamic-morphodynamic model Delft3D are compared with surf zone morphological change inferred from quarterly in-situ bathymetric surveys. The model gives plausible two-dimensional hydrodynamic predictions with offshore currents being strongest in the rip channels. When the default wave-induced bed-load transport is included the model predicts accretion on the bar similar to the observations but the predicted sandbar amplitude grows unrealistically. Both with and without wave-induced transport, the model underestimates the erosion in the rip channels.** [1]

I. Introduction

Understanding and predicting near-shore sediment transport and morphodynamics has important implications for civilian and naval coastal operations. The surf-zone sediment transport is forced by waves and wave-driven currents and the corresponding morphodynamic predictions involve coupled wave-hydrodynamic simulations. A highly resolved evolving bathymetry is generally needed in such simulations since the surf-zone currents can be strongly influenced by small bathymetric features such as rip-channels having a scale of about 100 m. Conventional in-situ methods for the acquisition of such high-resolution bathymetry are costly and take significant logistic efforts and time. A great promise for obtaining high-resolution near-shore bathymetry on operational time scale is provided by assimilating remote-sensing video observations [1,2] into a hydrodynamic model and solving an inverse problem for bathymetry [3].

Our objective is to develop a test case for further improvement of the inverse-model data-assimilation technique. In this study the emphasis is on longshore non-uniform hydrodynamic and morphodynamic patterns caused by rip-currents [4,5]. We use sediment transport hindcasts to calibrate the hydrodynamic predictions of the coupled wave-hydrodynamic-morphodynamic DELFT3D model. The calibration is based on comparison of the predicted bathymetric evolution with that inferred from high-resolution in-situ bathymetry surveys. The model focus area is a 2km stretch (Fig.1, red box) at Santa Rosa Island, Florida that is subject to hourly remote-sensing video observations from an ARGUS [2] station located at the origin; in-situ surveys are also routinely performed at this site. The test period is the summer of 2007 for which two in-situ surveys (Fig.2ab) indicate ±20 cm bathymetry changes consisting of erosion in the rip channels and some accretion over the bar. In the period between the two surveys the site was affected by a storm on August 22 with significant wave height H_S exceeding 1.5m (Fig.2c-e)

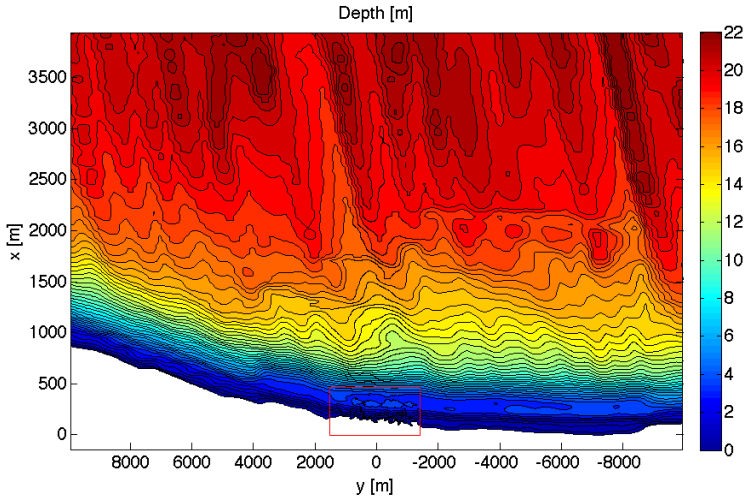

Fig.1 The computational domain and the respective initial bathymetry, composed of low-resolution coastal relief data and high resolution survey data. The red box encloses the focus area for the sediment transport hindcasts. The *x*-axis is stretched to emphasize the bar (~ 4m depth) and the high-resolution features inside the red box.

[1] Work sponsored by the Office of Naval Research for transition of capability related to surf zone bathymetry. J. Simeonov was supported through the ASEE NRL postdoctoral program.

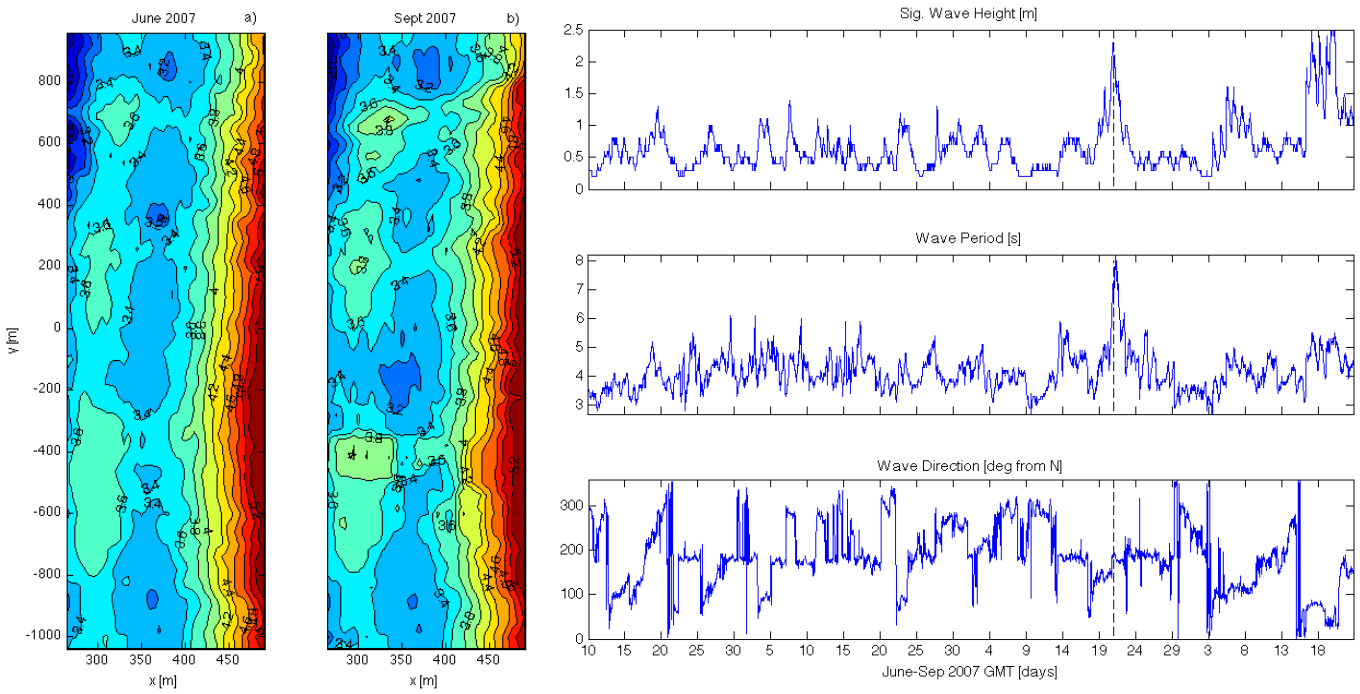

Fig.2 High-resolution 2007 bathymetry surveyed during June 10-12 (a) and September 10-12 (b) suggest erosion in the rip channels at y = -400m and accretion over the bar x = 350m, y = -200m. The bathymetry is accurate to ± 5cm. The significant wave height (c), wave period (d) and wave direction (e) for the period June 10 to September 23, 2007; data from NODC buoy 42039 in the Gulf of Mexico located some 100 miles south of the test site. The dashed line marks the August 22 storm with normally incident waves.

and normally incident waves. Such conditions can potentially give rise to strong rip currents and morphological changes characterized with non-uniform longshore variation. The effect of the August 22 storm on the surf zone bathymetry is illustrated by the ARGUS imagery in Fig. 3, where the initially longshore uniform breaker line develops kinks and gaps. The development of a very distinct gap (Fig. 3, fifth panel) located near the rip channel at y = - 450 (Fig. 2c) suggests that the August 22 storm may be partly responsible for the rip channel morphological change seen in Fig. 2a,b. Fig. 3 (last panel) also indicates that the breaker line returns to being longshore uniform after a September 17-20 storm with obliquely incident waves (Fig. 2c-e). The oblique waves usually produce longshore currents. Here, we make sediment transport hindcasts for stationary wave conditions with H_S = 2m approximately representing the August 22 storm with normally incident waves. To speed up the calibration process we consider only 12 hours of sediment transport. Because of the stationary conditions, these 12-hour simulations can be used to estimate bed changes over longer periods T using the multiplication factor of T/12.

II. Numerical Simulations

A. Model setup and initialization

We briefly discuss the setup used for the 2DH DELFT3D simulations. The model domain has its origin at the video tower (-86.766W, 30.3914N) approximately 100 m inland of the shore line and extends in the longshore (y) direction to y = ± 10 km; the cross-shore direction (x) is positive offshore varies between x = -150 m and x = 4000 m. The cross-shore boundaries are chosen sufficiently far from the area of primary interest near x, y = 0 in order to minimize the effect of boundary conditions. For this relatively large domain, we produced a composite bathymetry consisting of the June 2007 high-resolution survey data for x<600m, -1km < y < 1km (Fig.1, also Fig. 2a for details) and low-resolution bathymetry outside of this interval. Since the surf-zone bar is generally not resolved in the coastal relief data the low-resolution bathymetry is generated by merging the coastal relief data with various high-resolution survey data covering -9km < y < 4km. Non-uniform cross-/long-shore grid steps, increasing gradually from 5m/ 10m in the inner high-resolution region to 40m/100m in outer low-resolution region resulted in a computationally efficient grid with 328x400 grid nodes. Finally, some smoothing was applied in the y direction near the two ends at y = ± 10 km to further reduce the generation of undesirable boundary disturbances.

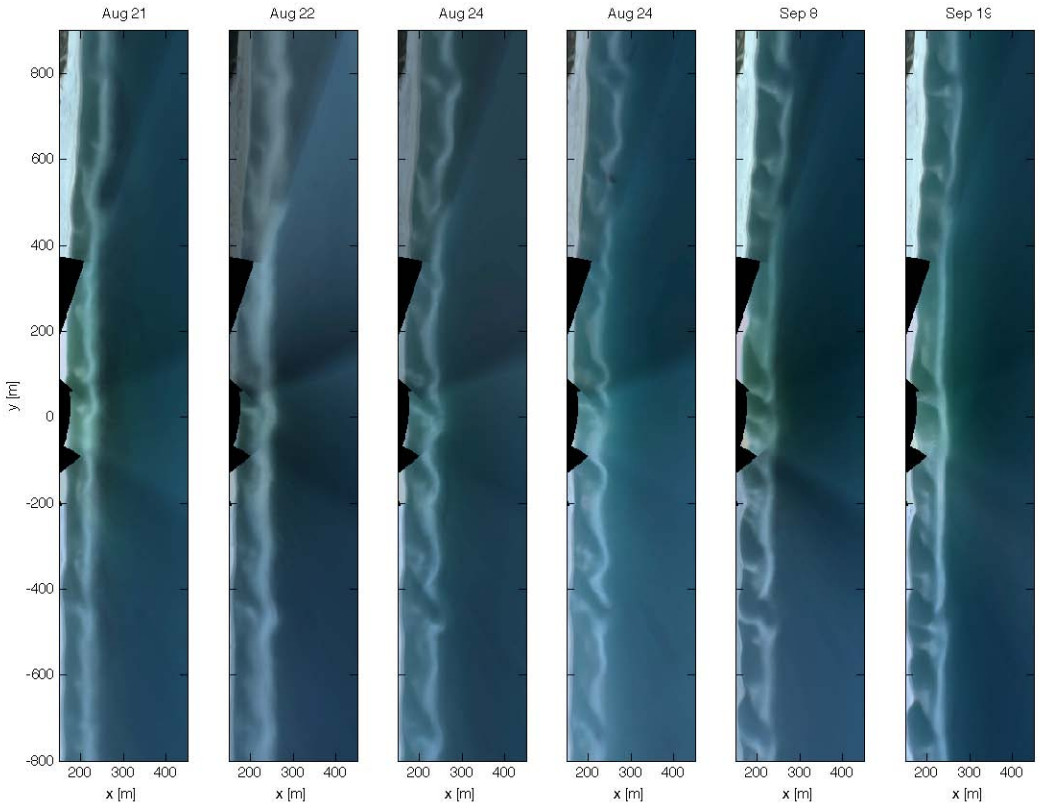

Fig.3 Time exposure ARGUS images from the model site show that the August 22 storm is associated with a transition (panels 1 through 5) from longshore uniform wave breaking to one characterized with quasi-periodic longshore variation. The wave breaking becomes longshore uniform (last panel) following the September 17-20 storm.

In the considered simulations, the currents are purely wave-driven and the forcing by wind is neglected. The radiation stress current forcing is computed using on-line coupling of the FLOW and the WAVE modules of the DELFT3D suite with a coupling interval of 60 min. The boundary condition for WAVE is a stationary wave energy spectrum obtained from an offshore ADCP buoy; the same uniform boundary condition is assumed on all three offshore boundaries. In the preliminary results given here we also assume a stationary boundary condition for the FLOW hydrodynamic simulations which consists of specifying a fixed sea level displacement η on the offshore boundary together with a zero sea level gradient $\partial\eta / \partial y = 0$ on the two cross-shore boundaries $y = \pm$ 10 km. Neglecting the tidal currents is justified on grounds of their relatively low magnitude, predominantly longshore direction and variation on length scales significantly larger than those of the rip channels. However, the tides can have a strong effect on the location of breakers by setting the overall depth of the water column. We include this effect below by considering different mean sea levels.

The time step for stable hydrodynamic integration is about 3 s and is limited by both advection and diffusion. The minimum cross-shore grid step Δx = 5m together with the assumed eddy diffusivity D = 6m^2/s gives the limit $\Delta t = \Delta x^2/D \approx$ 4s. The advective limit for a very strong cross-shore current u = 1.5 m/s is $\Delta t = \Delta x/u \approx$ 3s. Because of this small time step, a typical simulation of 12 hours model time takes about 2 days of CPU time. For the bottom drag we use mostly the Chezy formulation for the friction coefficient $r = g/C_{2D}^2$ where C_{2D} is the Chezy coefficient. The horizontal eddy viscosity was set to 1m^2/s and the WAVE calculations included the roller energy component. In all calculations we use a morphodynamic spin-up interval (fixed bed) of 2 hours; this seems to be acceptable under the present steady forcing where the currents tend to reach quisi-equilibrium in about 1 hour model time.

B. Results

The present morphodynamic simulations use the default DELFT3D sediment transport formulation of VanRijn [6] which includes three types of transport - bed-load transport due to mean currents, bed-load transport due to waves and suspended-load transport due to wave asymmetry. These three components can be calibrated in the model using the respective ad-hoc multiplication factors BED, BEDW and SUSW. Similarly, the magnitude of the suspended transport, computed from an advection-diffusion equation with sources and sinks, can be controlled by a multiplication factor SUS. The model sediment is sand with median grain diameter D50=0.3mm.

In our first test (Fig.4) we use the default values (1.0) for all four multiplication factors. Here we set the initial sea level and the water level boundary condition at η = - 30cm, corresponding to low-tide conditions. Under this condition the breakers and maximum rip-current intensity should be located the furthest in the offshore direction. In this and the following runs (unless noted otherwise) we consider a relatively strong bottom friction r = 0.04 (C_{2D}=18) which results in quasi-steady rip currents. Fig 4e shows that the maximum wave dissipation, peaking at 120 Wm^{-2}, is located at x = 400m, just offshore of the bar; significant wave dissipation also occurs in the shallow 1-2 m depths at x = 200m (onshore of the bar trough). The wave dissipation has a non-uniform long-shore distribution being maximum where the bar is the shallowest. The model rip currents resulting from the non-uniform wave dissipation distribution should also be coupled to the underlying bathymetry. Fig. 4a,c shows offshore directed flows in the two rip-channels at y = -400m and 200m (Fig.2a), but the model did not predict a rip current at the y = 700m channel. Fig. 4c-e suggest that the suspended sediment concentration, reaching a maximum of 0.08 kg/m^3 over the bar, is correlated with the strongest currents rather than the strongest wave dissipation. In this run, the sediment transport (not shown) is dominated by the wave-induced transport which is two orders of magnitude larger than the suspended transport by the currents. The wave-induced transport is directed onshore and its uniform longshore distribution results in the uniform accretion/erosion pattern on Fig. 4f. The maximum accretion takes place over the bar which seems to agree with the surveys (Fig. 2a,b), but the simulated accretion magnitude of 50cm per 12 hours overpredicts the observed one.

To test whether the observed non-uniform accretion/deposition pattern can be explained by sediment transport solely due to rip currents we next make a simulation (Fig.5) with BEDW=SEDW=0, keeping the rest of the setup the same as in the previous run. This setting results in negligible bed-load transport (not shown) so that the total transport was entirely due to suspended transport by the currents. Because the considered depth changes are small and the forcing is unchanged, the predicted wave dissipation pattern (Fig. 5e) and currents (Fig. 5a-c) differ little from those in Fig.4. The spatial distribution of the respective sediment concentration field (Fig.5d) is also similar to that in Fig.4, but the maximum concentration over the bar 0.06 kg/m^3 is smaller. Unlike the previous run, the predicted bed changes (Fig. 5f) are noticeably non-uniform in the longshore direction and consist mainly of erosion offshore of the bar. The predicted erosion magnitude was an order of magnitude smaller than that in the previous run.

Th run in Fig.5 is next repeated with initial and boundary sea level set at η = 30 cm to model the effect of increased water depth at high tide. As expected, the predicted wave dissipation over the bar (not shown) is much weaker (less than 100 Wm^{-2}) but the predicted erosion pattern is essentially the same as that in Fig.5 except that the erosion magnitude was 20% smaller. Thus, including varying sea level due to tides does not seem to result in qualitatively different morphodynamic patterns. The run in Fig.5 is also repeated with reduced and spatially variable bottom friction using the Manning formulation for the Chezy coefficient

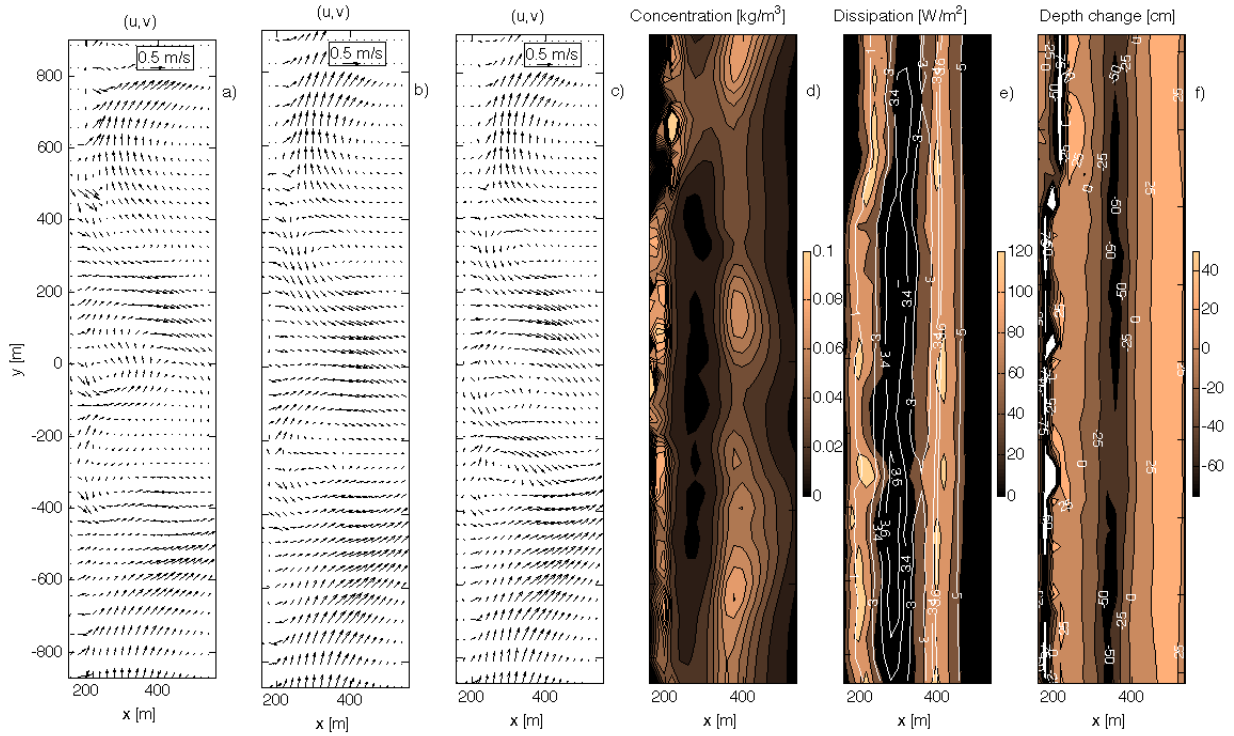

Fig.4 The simulated flow field at three times t = 2 (a), 7 (b) and 12 (c) hours in the first run with default sediment transport multiplication factors and low-tide sea level = -0.3m. Concentration d), wave energy dissipation e) and total depth change f) at t=12 hours. Selected depth contours (white) are also given in e). Bed erosion is positive in f).

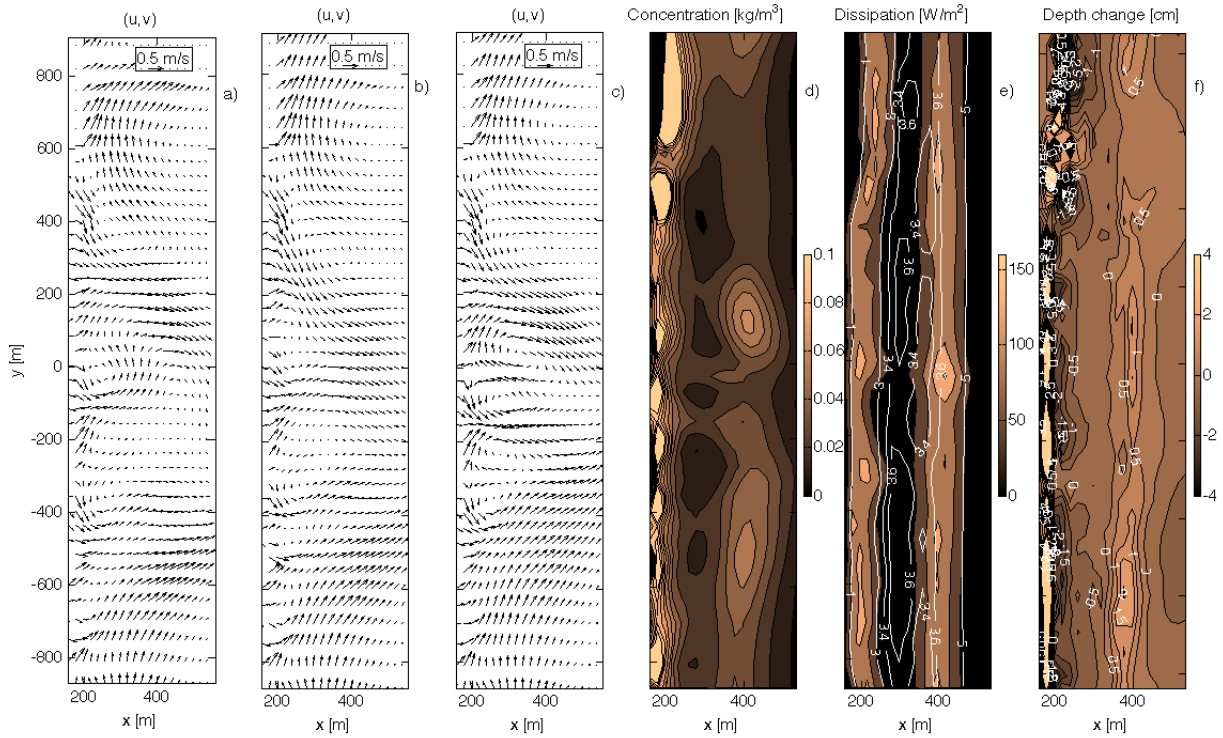

Fig.5 The simulated flow field at three times t = 2 (a), 7 (b), and 12 (c) hours in the run with SUSW=BEDW=0 and low-tide sea level = -0.3m. Concentration d), wave energy dissipation e) and total depth change f) at t=12 hours. Selected depth contours (white) are also given in e). Bed erosion is positive in f).

$C_{2D} = H^{1/6} / n$, where H is the water depth and n is the Manning coefficient. In this final run we use n = 0.03 which results in bottom friction varying from r = 0.13 at H = 0.5m to r = 0.0056 at H = 4m. The reduced bottom friction resulted in more variable rip currents near the shoreline but the current magnitude over the bar and the associated erosion magnitude remained unchanged.

The model skill in predicting rip currents is further illustrated in Fig. 6 by plotting the longshore variation of the current direction $cos(a)$ relative to the x-axis and the current offshore component for different bottom friction r and water depth η. In all three cases, the current magnitude and direction are strongly correlated with the position of the rip channel (Fig.6 dashed lines). All three runs also predict rip currents with essentially the same magnitude of the offshore flow equal to about 0.22 m/s. On Fig.7

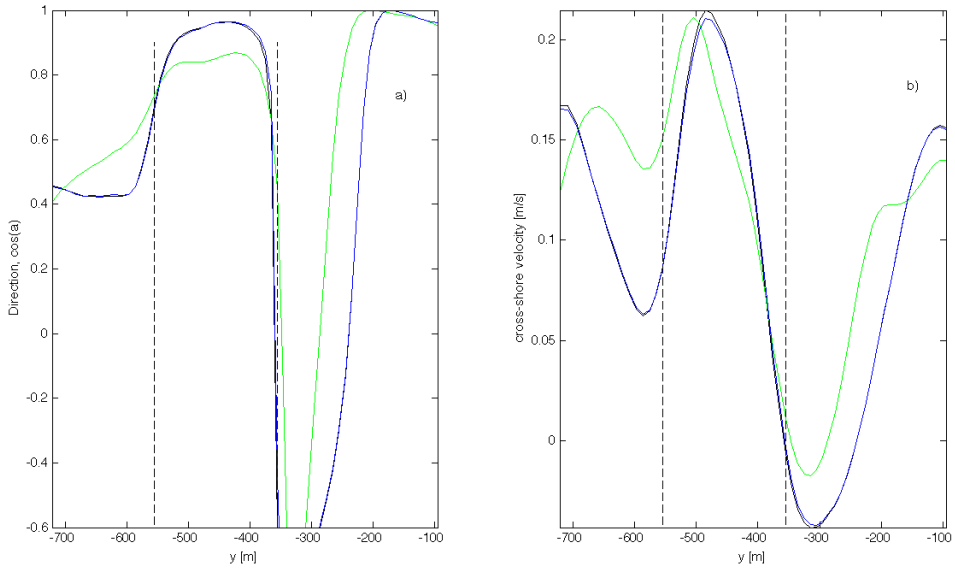

Fig.6 Longshore cross-sections (x=257m) of the current direction (a) and the offshore magnitude of the current (b) for r = 0.04 and η = -0.3 (black), r = 0.04 and η = +0.3 (green), and n= 0.03 (variable r) and η = -0.3 (blue). Vertical dashes denote the width of the y=-450m rip channel.

we present cross-shore bathymetry profiles at two different *y* locations to facilitate model-to-model and model-to-observation comparison. Note, that we can make only qualitative comparison to observations because the period between the two surveys is much larger than 12 hours and includes various wave conditions. Outside the rip channels, at *y* = -200 (Fig.7a) the run with wave-induced sediment transport (blue) predicts accretion in agreement with the observed bathymetry change (dashed). However, this run predicts accretion also in the *y* = -450 rip channel (Fig.7b, blue) which disagrees with the survey bathymetry (dashed). The run with the sediment transport due to currents only (red) generally gives bathymetry changes of 1-2 cm that are too small to account for the observations.

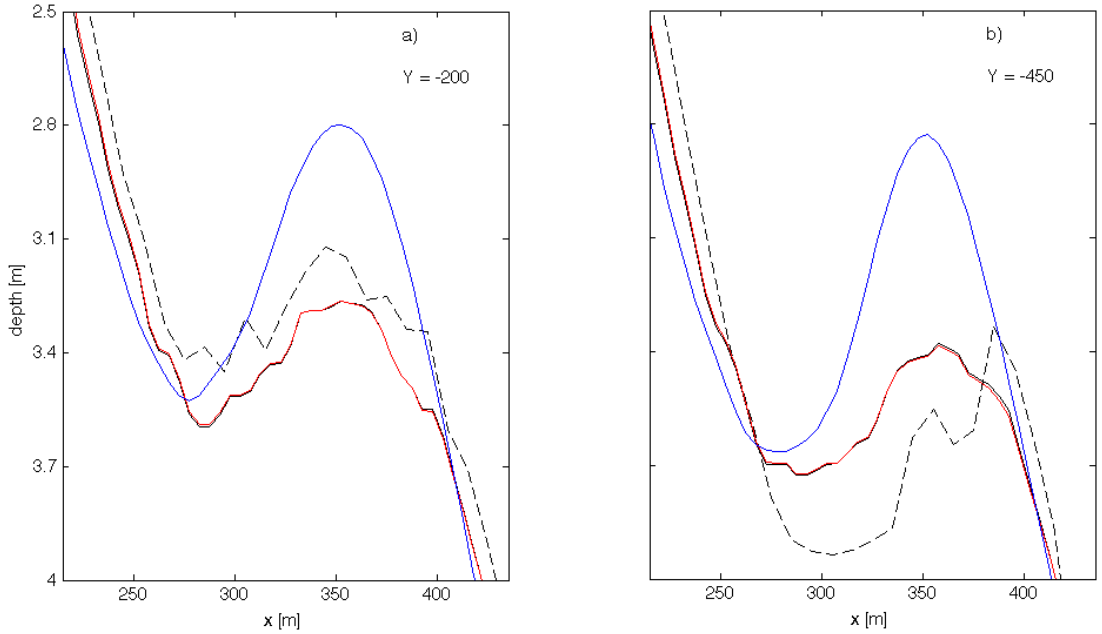

Fig.7 Cross-shore sections of the model and observed bathymetry at *y* = -200 (a) and *y* = -450 (b): the initial June 2007 bathymetry (solid black), at the end of run in Fig. 4 with wave-induced transport (blue), at the end of run in Fig. 5 without wave induced transport (red) and the observed September 2007 bathymetry (dashed black).

III. CONCLUSIONS

We have performed sediment transport hindcasts for the purpose of calibrating the DELFT3D morphodynamic model against observations of evolving rip channel bathymetry at Santa Rosa Island, Florida. The hindcasts were limited to quasi-steady hydrodynamic conditions by using a relatively strong bottom friction and by assuming stationary water level (no tides) and wave forcing corresponding to a storm event with normally incident waves. The results indicate that the default DELFT3D sediment transport formulation which includes wave-induced transport overpredicts the observed accretion on the bar and fails to reproduce the observed deepening in the rip channels. The wave-induced transport was then suppressed to estimate morphodynamics involving only suspended transport by currents. With the relatively weak depth-averaged model currents it was found that the predicted suspended transport is too small to account for the observed erosion/accretion magnitude. To obtain stronger currents and larger suspended transport rates it may be necessary to further reduce the bottom friction and to include undertow. The latter will requires fully three-dimensional modeling. Future work will also consider non-stationary wave and tidal forcing using the observed time series.

ACKNOWLEDGMENT

The authors would like to thank K. Edwards, L. Hsu and J. Veeramony for helpful discussions.

REFERENCES

[1] K.T. Holland, R.A. Holman, T.C. Lippmann, J. Stanley and N. Plant, "Practical use of video imagery in nearshore oceanographic field studies," *IEEE Journal of Oceanic Engineering*, vol. 22(1), pp. 81-92, 1997.

[2] R.A Holman and J. Stanley,"The history and technical capabilities of Argus," *Coastal Engineering*, vol. 54, pp. 477-491, 2007.

[3] A. Van Dongeren et al., "Beach Wizard: Nearshore bathymetry estimation through assimilation of model computations and remote observations," *Coastal Engineering*, vol. 55, pp. 1016-1027, 2008.

[4] A.J.H.M. Reniers, J.A. Roelvink and E.B. Thornton, "Morphodynamic modeling of an embayed beach under wave group forcing," *Journal of Geophysical Research*, vol. 109, C01030, doi: 10:1029/2002JC001586, 2004.

[5] J.N. Damgaard, N. Dodd, L. Hall and T. Chester, "Morphodynamic modeling of rip channel growth," *Coastal Engineering*, vol. 45, pp. 199-221, 2002.

[6] L.C. Van Rijn, "Principles of sediment transport in rivers, estuaries and coastal seas," *Aqua Publications*, Amsterdam, 1993.